Nonreciprocal Dyakonov-wave propagation supported by topological insulators

Journal of the Optical Society of America B
OPTICAL PHYSICS

Nonreciprocal Dyakonov-wave propagation supported by topological insulators

Tom G. Mackay[1,2,*] and Akhlesh Lakhtakia[2]

[1]School of Mathematics and Maxwell Institute for Mathematical Sciences, University of Edinburgh, Edinburgh EH9 3FD, UK
[2]Department of Engineering Science and Mechanics, Pennsylvania State University, University Park, Pennsylvania 16802-6812, USA
*Corresponding author: T.Mackay@ed.ac.uk

Received 24 March 2016; revised 28 April 2016; accepted 2 May 2016; posted 3 May 2016 (Doc. ID 261823); published 25 May 2016

The propagation of Dyakonov waves guided by the planar interface of a columnar thin film and a topological insulator was investigated by numerically solving the associated canonical boundary-value problem. The topological insulator was modeled as an isotropic dielectric material endowed with a nonzero surface admittance. The propagation directions for the Dyakonov waves, as well as the decay constants and phase speeds of the waves, were significantly modulated by varying the magnitude of the surface admittance. Most significantly, a Dyakonov wave propagating along the direction of a vector $\underline{u}$ has a different phase speed and different decay constants as compared with the Dyakonov wave which propagates along the direction of $-\underline{u}$. This nonreciprocity, with respect to interchanging the direction of Dyakonov-wave propagation, is not exhibited when the topological insulator is replaced by an isotropic dielectric material of the same refractive index but with a nonzero surface conductivity instead of a surface admittance.

OCIS codes: (240.6690) Surface waves; (260.2110) Electromagnetic optics; (260.1180) Crystal optics.

http://dx.doi.org/10.1364/JOSAB.33.001266

1. INTRODUCTION

The discovery of topological insulators [1], such as the chalcogenides Bi_2Se_3, Bi_2Te_3, and Sb_2Te_3, has prompted a flurry of research activity, much of which has been directed toward revealing their optical properties [2–4]. To this end, the theory underpinning optical scattering from spheres made of topological insulators was recently developed [5]. Classically, a topological insulator may be modeled as an achiral biisotropic material whose nonreciprocity is captured by a magnetoelectric pseudoscalar γ [6]. Alternatively, a topological insulator may be regarded as an isotropic dielectric–magnetic material whose surface is endowed with a surface admittance γ. These two different models give rise to identical results in terms of optical scattering [7]. Macroscopically, topological insulation is a surface phenomenon manifesting as protected conducting states that exist at the surface, but not in the bulk, of a topological insulator [1,2]. Therefore, we adopted the latter model in this paper.

Electromagnetic plane waves bound to the surface of a topological insulator are investigated here. Previous studies in this area have focused upon surface-plasmon-polariton waves [8–12]. In contrast, we investigate Dyakonov waves guided by the planar interface of a topological insulator and an anisotropic dielectric material [13,14]. While Dyakonov-wave propagation guided by the planar interface of two homogeneous dielectric materials, one isotropic and the other anisotropic, is possible only for a very small range of propagation directions, these surface waves offer considerable potential for long-range on-chip communication [15]. Parenthetically, let us note the dramatic enlargement of the range of propagation directions if the anisotropic partnering material is either a hyperbolic material [16,17] or a periodically nonhomogeneous material [18], but the range-enlargement issue lies outside the scope of this paper.

The anisotropic dielectric material is taken to be a columnar thin film (CTF) [19,20] here. CTFs may be effectively regarded as orthorhombic biaxial materials for optical purposes. Their optical properties and porosity may be engineered through judicious control of the vapor deposition technique used for their fabrication. Dyakonov waves are studied by solving the corresponding canonical boundary-value problem [21] in which the topological insulator occupies the half-space $z < 0$ while the CTF occupies the half-space $z > 0$. We contrast the characteristics of Dyakonov waves at the CTF/topological insulator interface with the characteristics of Dyakonov waves at the interface of a CTF and an isotropic dielectric material whose bulk properties are the same as the topological insulator but whose surface is endowed by a surface conductivity $\tilde{\sigma}$ [22] instead of the surface admittance γ.

2. BOUNDARY-VALUE PROBLEM FOR DYAKONOV-WAVE PROPAGATION

A schematic diagram illustrating the growth of a CTF by vapor deposition is provided in Fig. 1. The parallel columns grow on a

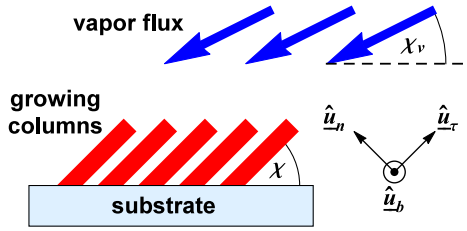

Fig. 1. Schematic representation of the growth of a CTF.

substrate that is oriented parallel to the xy plane. The angle between the growing columns and the substrate plane is χ, while the angle between the incident vapor flux and the xy plane is $\chi_v \leq \chi$. Without loss of generality, Dyakonov-wave propagation parallel to the x axis in the xy plane is considered. The orientation of the CTF's morphologically significant plane relative to the direction of Dyakonov-wave propagation is specified by the angle ψ, as is schematically illustrated in Fig. 2. Accordingly, the relative permittivity dyadic of the CTF is expressed as

$$\underline{\underline{\epsilon}}_{\text{CTF}} = n_a^2 \hat{\underline{u}}_n \hat{\underline{u}}_n + n_b^2 \hat{\underline{u}}_\tau \hat{\underline{u}}_\tau + n_c^2 \hat{\underline{u}}_b \hat{\underline{u}}_b, \tag{1}$$

wherein $n_{a,b,c}$ are the principal refractive indexes, and the unit vectors

$$\left.\begin{aligned} \hat{\underline{u}}_n &= -(\hat{\underline{u}}_x \cos\psi + \hat{\underline{u}}_y \sin\psi)\sin\chi + \hat{\underline{u}}_z \cos\chi \\ \hat{\underline{u}}_\tau &= (\hat{\underline{u}}_x \cos\psi + \hat{\underline{u}}_y \sin\psi)\cos\chi + \hat{\underline{u}}_z \sin\chi \\ \hat{\underline{u}}_b &= \hat{\underline{u}}_x \sin\psi - \hat{\underline{u}}_y \cos\psi \end{aligned}\right\} \tag{2}$$

are expressed in terms of the standard Cartesian unit basis vectors $\{\hat{\underline{u}}_x, \hat{\underline{u}}_y, \hat{\underline{u}}_z\}$. The substrate is an isotropic dielectric material specified by the refractive index n_s.

Let $\underline{\mathcal{E}}_\ell$ and $\underline{\mathcal{H}}_\ell$ denote the (complex-valued) electric and magnetic field phasors, respectively, of angular frequency ω, with $\ell = c$ for the region $z > 0$ and $\ell = s$ for the region $z < 0$. According to the Maxwell curl postulates, the phasors satisfy

$$\left.\begin{aligned} \underline{k}_c \times \underline{\mathcal{E}}_c &= \omega\mu_0 \underline{\mathcal{H}}_c \\ \underline{k}_c \times \underline{\mathcal{H}}_c &= -\omega\epsilon_0 \underline{\underline{\epsilon}}_{\text{CTF}} \cdot \underline{\mathcal{E}}_c \end{aligned}\right\} \tag{3}$$

in the region $z > 0$, where ϵ_0 and μ_0 are the free-space permittivity and permeability, respectively. The wave vector

$$\underline{k}_c = k_0(\varkappa \hat{\underline{u}}_x + i q_c \hat{\underline{u}}_z), \tag{4}$$

wherein $k_0 = \omega\sqrt{\epsilon_0\mu_0}$ is the free-space wavenumber. The propagation constant $\varkappa > 0$ for Dyakonov-wave propagation directed along the positive x axis, whereas $\varkappa < 0$ for Dyakonov-wave propagation directed along the negative x axis. Furthermore, the real part of the decay constant q_c must be positive valued. As described in detail elsewhere [23], the values of q_c are determined by combining Eqs. (3) and (4). This provides a system of homogeneous equations that are linear in the six components of $\underline{\mathcal{E}}_c$ and $\underline{\mathcal{H}}_c$; the determinant of this system delivers a quartic polynomial, the roots of which yield four values of q_c. The two roots conforming to $\text{Re}[q_c] > 0$ are selected and denoted as q_{c1} and q_{c2}. The two corresponding wave vectors for the region $z > 0$ are denoted as $\underline{k}_{c1}$ and $\underline{k}_{c2}$. Thus, the phasors for $z > 0$ may be expressed as

$$\left.\begin{aligned} \underline{\mathcal{E}}_c &= A_{c1}\underline{\mathcal{E}}_{c1} + A_{c2}\underline{\mathcal{E}}_{c2} \\ \underline{\mathcal{H}}_c &= \tfrac{1}{\omega\mu_0}(A_{c1}\underline{k}_{c1} \times \underline{\mathcal{E}}_{c1} + A_{c2}\underline{k}_{c1} \times \underline{\mathcal{E}}_{c2}) \end{aligned}\right\}, \tag{5}$$

wherein $\underline{\mathcal{E}}_{c1,c2}$ arise from Eqs. (3) and (4) as eigenvectors corresponding to $\underline{k}_{c1,c2}$ [23].

According to the Maxwell curl postulates, the phasors satisfy

$$\left.\begin{aligned} \underline{k}_s \times \underline{\mathcal{E}}_s &= \omega\mu_0 \underline{\mathcal{H}}_s \\ \underline{k}_s \times \underline{\mathcal{H}}_s &= -\omega\epsilon_0 n_s^2 \underline{\mathcal{E}}_s \end{aligned}\right\} \tag{6}$$

in the $z < 0$ region, where the wave vector

$$\underline{k}_s = k_0(\varkappa \hat{\underline{u}}_x - i q_s \hat{\underline{u}}_z), \tag{7}$$

with the decay constant $q_s = \sqrt{\varkappa^2 - n_s^2}$ conforming to $\text{Re}[q_s] > 0$ for Dyakonov-wave propagation. Solutions to Eq. (6) are represented by

$$\left.\begin{aligned} \underline{\mathcal{E}}_s &= A_{s1}\hat{\underline{u}}_y + A_{s2}(i q_s \hat{\underline{u}}_x + \varkappa \hat{\underline{u}}_z) \\ \underline{\mathcal{H}}_s &= \sqrt{\tfrac{\epsilon_0}{\mu_0}}[A_{s1}(i q_s \hat{\underline{u}}_x + \varkappa \hat{\underline{u}}_z) - A_{s2} n_s^2 \hat{\underline{u}}_y] \end{aligned}\right\}. \tag{8}$$

The scalar amplitude coefficients $A_{c1,c2}$ and $A_{s1,s2}$ introduced in Eqs. (5) and (8), respectively, are related by the following boundary conditions imposed at the interface $z = 0$. Two cases are considered: in case (i) the substrate possesses topologically insulating surface states characterized by the surface admittance γ [7], while in case (ii) the substrate possesses a surface charge characterized by the surface conductivity $\tilde{\sigma}$ [22,24,25]. Accordingly, the boundary conditions for case (i) may be formulated as

$$\left.\begin{aligned} \hat{\underline{u}}_z \times (\underline{\mathcal{E}}_c - \underline{\mathcal{E}}_s) &= \underline{0} \\ \hat{\underline{u}}_z \times (\underline{\mathcal{H}}_c - \underline{\mathcal{H}}_s) &= -\gamma \hat{\underline{u}}_z \times \underline{\mathcal{E}}_s \end{aligned}\right\}, \tag{9}$$

while those for case (ii) may be formulated as

$$\left.\begin{aligned} \hat{\underline{u}}_z \times (\underline{\mathcal{E}}_c - \underline{\mathcal{E}}_s) &= \underline{0} \\ \hat{\underline{u}}_z \times (\underline{\mathcal{H}}_c - \underline{\mathcal{H}}_s) &= \tilde{\sigma}(\hat{\underline{u}}_x \hat{\underline{u}}_x + \hat{\underline{u}}_y \hat{\underline{u}}_y) \cdot \underline{\mathcal{E}}_s \end{aligned}\right\}. \tag{10}$$

Because Eqs. (9) and (10) each yield a system of four homogeneous equations that are linear in the scalar amplitude coefficients $A_{c1,c2}$ and $A_{s1,s2}$, each may be expressed conveniently in the matrix-vector form

$$[M] \cdot [A_{s1} \quad A_{s2} \quad A_{c1} \quad A_{c2}]^T = [0 \quad 0 \quad 0 \quad 0]^T. \tag{11}$$

Thus, the dispersion relations for Dyakonov-wave propagation for cases (i) and (ii) are represented by

$$\det[M] = 0, \tag{12}$$

with $[M]$ being the 4×4 matrix introduced in Eq. (11). The complexity of Eq. (12) is such that an algebraic solution is

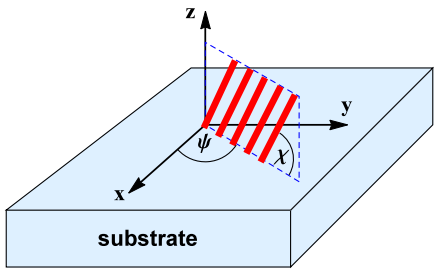

Fig. 2. Orientation of the CTF's morphologically significant plane.

impractical. Accordingly, recourse was taken to a numerical investigation of Eq. (12).

3. NUMERICAL STUDIES

For our computations, the CTF was taken to be made from titanium dioxide. The following are experimentally determined values of the principal refractive indexes for such a CTF at a free-space wavelength of 633 nm [19]:

$$\left.\begin{aligned} n_a &= 1.0443 + 2.7394(2\chi_v/\pi) - 1.3697(2\chi_v/\pi)^2 \\ n_b &= 1.6765 + 1.5649(2\chi_v/\pi) - 0.7825(2\chi_v/\pi)^2 \\ n_c &= 1.3586 + 2.1109(2\chi_v/\pi) - 1.0554(2\chi_v/\pi)^2 \end{aligned}\right\}, \quad (13)$$

with $\tan\chi = 2.8818\tan\chi_v$, where the columnar inclination angle χ and vapor flux angle χ_v (see Fig. 1) are given in radians. We fixed the vapor flux angle $\chi_v = 19.1°$ and the refractive index of the substrate $n_s = 1.8$.

For a given value of γ or $\tilde{\sigma}$, Eq. (12) was solved to determine the values of ψ for which Dyakonov-wave propagation is possible [23]. In fact, for $\gamma = \tilde{\sigma} = 0$, four narrow ranges of ψ are found to support Dyakonov-wave propagation: $\psi \in [\pm\psi_m - \Delta\psi/2, \pm\psi_m + \Delta\psi/2]$ and $\psi \in [180° \pm \psi_m - \Delta\psi/2, 180° \pm \psi_m + \Delta\psi/2]$. For case (i), we found that the values of ψ for which Dyakonov-wave propagation is possible depend upon the sign of $\varkappa$. In contrast, the values of ψ for which Dyakonov-wave propagation is possible do not depend upon the sign of $\varkappa$ for case (ii).

The angle ψ_m, which represents the midpoint of the ψ range that supports Dyakonov-wave propagation, is plotted against (i) $\eta_0\gamma/\tilde{\alpha}$ and (ii) $\eta_0\tilde{\sigma}/\tilde{\alpha}$ in Fig. 3. Here, $\eta_0 = \sqrt{\mu_0/\epsilon_0}$ is the free-space impedance, while $\tilde{\alpha} = 7.297352566 \times 10^{-3}$ is the fine structure constant [26]. The range of γ values reflects a hopeful future for the presently infant field of topological insulators that could grow to encompass mixed materials and new material compositions. For case (i), the midpoint angle ψ_m increases uniformly as γ increases for $\varkappa > 0$ whereas ψ_m decreases uniformly as γ increases for $\varkappa < 0$. For case (ii), the midpoint angle ψ_m increases uniformly as $\tilde{\sigma}$ increases, at a substantially faster rate than the corresponding rate of increase for the topological insulator case with $\varkappa > 0$. The value of ψ_m for $\gamma = 0$, regardless of the sign of $\varkappa$, is the same as it is for $\tilde{\sigma} = 0$, as may be anticipated from Eqs. (9) and (10).

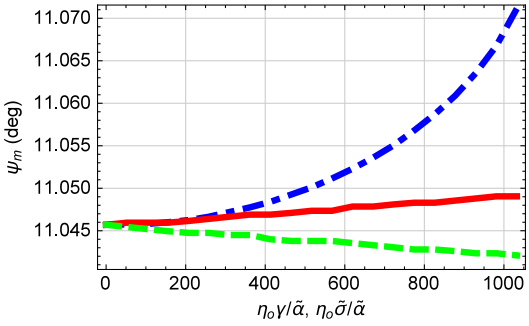

Fig. 3. ψ_m (deg) plotted against $\eta_0\gamma/\tilde{\alpha}$ for $\varkappa > 0$ (solid, red curve) and $\varkappa < 0$ (dashed, green curve), and against $\eta_0\tilde{\sigma}/\tilde{\alpha}$ (broken dashed, blue curve).

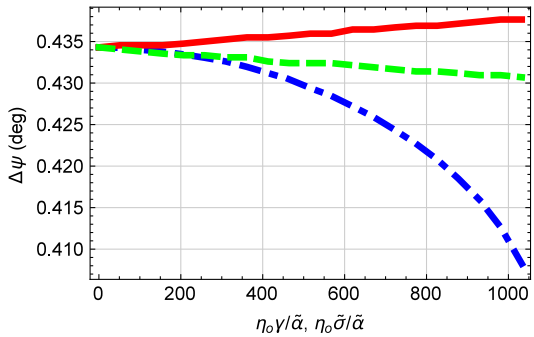

Fig. 4. As Fig. 3 but with $\Delta\psi$ (deg) on the vertical axis.

The extent of the angular range for which Dyakonov-wave propagation is possible, namely, $\Delta\psi$, is plotted against (i) $\eta_0\gamma/\tilde{\alpha}$ and (ii) $\eta_0\tilde{\sigma}/\tilde{\alpha}$ in Fig. 4. For case (i), the magnitude of $\Delta\psi$ increases uniformly as γ increases for $\varkappa > 0$ whereas $\Delta\psi$ decreases uniformly as γ increases for $\varkappa < 0$. For case (ii), the magnitude of $\Delta\psi$ decreases uniformly as $\tilde{\sigma}$ increases, at a substantially faster rate than the corresponding rate of decrease for the topological insulator case with $\varkappa < 0$.

Let $k_0 m$ be the wavenumber for plane-wave propagation in the bulk CTF. In general, two distinct values of m are possible, which arise as roots of the equation [23,27]

$$\frac{n_b^2\cos^2\chi\cos^2\psi}{m^2 - n_b^2} + \frac{n_c^2\sin^2\psi}{m^2 - n_c^2} + \frac{n_a^2\sin^2\chi\cos^2\psi}{m^2 - n_a^2} = 0. \quad (14)$$

Let $m_{\max}$ denote the larger of these two roots. Then, the magnitude of the Dyakonov wave's phase speed relative to the lower in magnitude of the two phase speeds in the bulk CTF is provided by $\overline{v} = m_{\max}/\varkappa$. Furthermore, let $\overline{v}_{\text{ave}}$ represent the average of the two values of $\overline{v}$ at $\psi = \psi_m \pm \Delta\psi$. The scaled logarithm of $\overline{v}_{\text{ave}}$ is plotted against (i) $\eta_0\gamma/\tilde{\alpha}$ and (ii) $\eta_0\tilde{\sigma}/\tilde{\alpha}$ in Fig. 5. For case (i), $\overline{v}_{\text{ave}}$ increases uniformly as γ increases

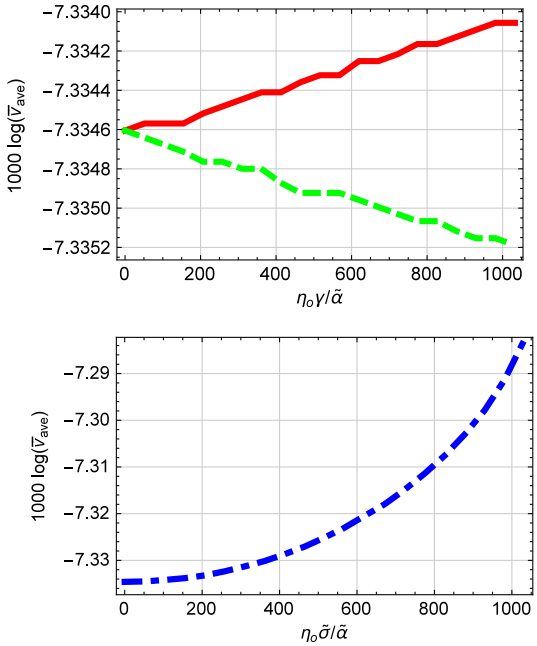

Fig. 5. As Fig. 3 but with 1000 log($\overline{v}_{\text{ave}}$) on the vertical axes.

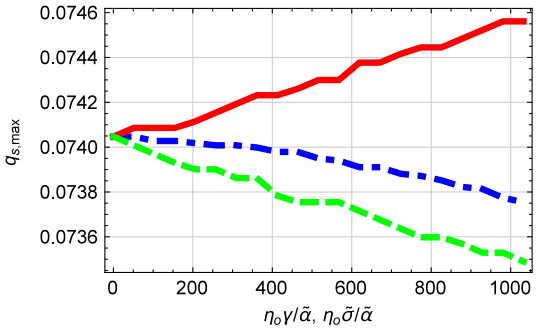

Fig. 6. As Fig. 3 but with $q_{s,\max}$ on the vertical axis.

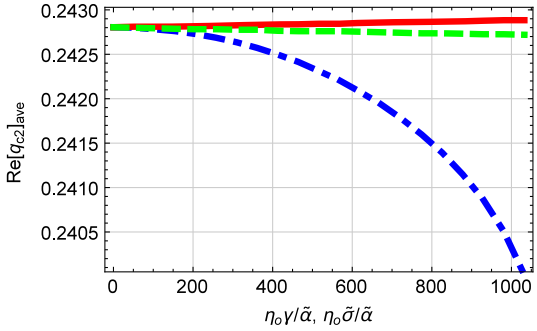

Fig. 8. As Fig. 3 but with $\mathrm{Re}[q_{c2}]_{\mathrm{ave}}$ on the vertical axis.

for $\varkappa > 0$ whereas $\overline{v}_{\mathrm{ave}}$ decreases uniformly as γ increases for $\varkappa < 0$. For case (ii), $\overline{v}_{\mathrm{ave}}$ increases uniformly as $\tilde{\sigma}$ increases, at a substantially faster rate than the corresponding rate of increase for the topological insulator case with $\varkappa > 0$. Notice that $\overline{v}_{\mathrm{ave}} < 1$ for all values of γ and $\tilde{\sigma}$.

The extent to which Dyakonov waves are bound to the CTF/substrate interface is gauged by the real parts of the decay constants q_s and $q_{c1,c2}$. In the region $z < 0$, the decay constant q_s is real valued. Whereas $q_s \to 0$ as $\psi \to \psi_m - \Delta\psi/2$, the maximum value $q_{s,\max}$ of q_s is attained in the limit $\psi \to \psi_m + \Delta\psi/2$. In Fig. 6, $q_{s,\max}$ is plotted against (i) $\eta_0\gamma/\tilde{\alpha}$ and (ii) $\eta_0\tilde{\sigma}/\tilde{\alpha}$. For case (i), $q_{s,\max}$ for $\varkappa > 0$ increases uniformly as γ increases, whereas $q_{s,\max}$ decreases uniformly as γ increases for $\varkappa < 0$. For case (ii), $q_{s,\max}$ decreases uniformly as $\tilde{\sigma}$ increases, at a noticeably slower rate than the corresponding rate of decrease for the topological insulator case with $\varkappa < 0$.

In the region $z > 0$, the decay constants $q_{c1,c2}$ are complex valued. Whereas $\mathrm{Re}[q_{c1}] \to 0$ as $\psi \to \psi_m + \Delta\psi/2$, the maximum value $\mathrm{Re}[q_{c1}]_{\max}$ of $\mathrm{Re}[q_{c1}]$ is attained in the limit $\psi \to \psi_m - \Delta\psi/2$. In Fig. 7, $\mathrm{Re}[q_{c1}]_{\max}$ is plotted against (i) $\eta_0\gamma/\tilde{\alpha}$ and (ii) $\eta_0\tilde{\sigma}/\tilde{\alpha}$. For case (i), $\mathrm{Re}[q_{c1}]_{\max}$ is independent of γ regardless of the sign of $\varkappa$. For case (ii), $\mathrm{Re}[q_{c1}]_{\max}$ decreases uniformly as $\tilde{\sigma}$ increases.

Unlike the behavior of $\mathrm{Re}[q_{c1}]$, there is little variation in the magnitude of $\mathrm{Re}[q_{c2}]$ across the ψ range for Dyakonov-wave propagation. Let $\mathrm{Re}[q_{c2}]_{\mathrm{ave}}$ denote the average of the two values of $\mathrm{Re}[q_{c2}]$ at $\psi = \psi_m \pm \Delta\psi$. In Fig. 8, $\mathrm{Re}[q_{c2}]_{\mathrm{ave}}$ is plotted against (i) $\eta_0\gamma/\tilde{\alpha}$ and (ii) $\eta_0\tilde{\sigma}/\tilde{\alpha}$. For case (i), $\mathrm{Re}[q_{c2}]_{\mathrm{ave}}$ for $\varkappa > 0$ increases uniformly as γ increases whereas $\mathrm{Re}[q_{c2}]_{\mathrm{ave}}$ decreases uniformly as γ increases for $\varkappa < 0$. For case (ii), $\mathrm{Re}[q_{c2}]_{\mathrm{ave}}$ decreases uniformly as $\tilde{\sigma}$ increases, at a substantially faster rate than the corresponding rate of decrease for the topological insulator case with $\varkappa < 0$.

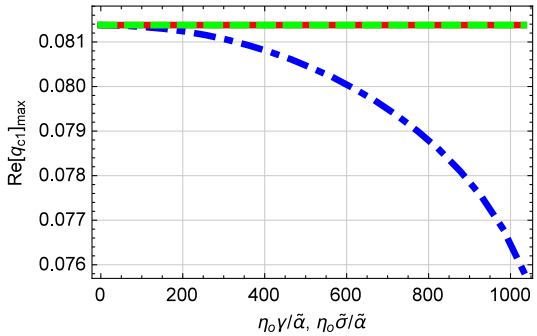

Fig. 7. As Fig. 3 but with $\mathrm{Re}[q_{c1}]_{\max}$ on the vertical axis.

4. CLOSING REMARKS

In conclusion, the directions along which Dyakonov waves propagate at the planar interface of a CTF and a topological insulator are significantly modulated by varying the magnitude of the topological insulator's surface admittance γ; so too are the decay constants and phase speeds of these Dyakonov waves. Values of $\gamma\eta_0/\tilde{\alpha}$ other than ± 1 require the use of magnetic coatings and/or immersion in a magnetostatic field [6]. Most importantly, a Dyakonov wave propagating along the direction of a vector $\underline{u}$ has a different phase speed and different decay constants as compared with the Dyakonov wave which propagates along the direction of $-\underline{u}$. This nonreciprocity, with respect to interchanging the direction of Dyakonov-wave propagation, is not exhibited when the topological insulator is replaced by an isotropic dielectric material of the same refractive index but with a surface conductivity $\tilde{\sigma}$ instead of a surface admittance γ. Dyakonov-wave propagation thus provides a way to distinguish between topologically insulating surface states and conducting surface states.

Funding. Engineering and Physical Sciences Research Council (EPSRC) (EP/M018075/1); Charles Godfrey Binder Endowment.

REFERENCES

1. M. Z. Hasan and C. L. Kane, "Topological insulators," Rev. Mod. Phys. **82**, 3045–3067 (2010).
2. M.-C. Chang and M.-F. Yang, "Optical signature of topological insulators," Phys. Rev. B **80**, 113304 (2009).
3. F. Liu, J. Xu, G. Song, and Y. Yang, "Goos-Hänchen and Imbert-Fedorov shifts at the interface of ordinary dielectric and topological insulator," J. Opt. Soc. Am. B **30**, 735–741 (2013).
4. F. Liu, J. Xu, and Y. Yang, "Polarization conversion of reflected electromagnetic wave from topological insulator," J. Opt. Soc. Am. B **31**, 735–741 (2014).
5. A. Lakhtakia and T. G. Mackay, "Electromagnetic scattering by homogeneous, isotropic, dielectric-magnetic sphere with topologically insulating surface states," J. Opt. Soc. Am. B **33**, 603–609 (2016).
6. X.-L. Qi, T. L. Hughes, and S.-C. Zhang, "Topological field theory of time-reversal invariant insulators," Phys. Rev. B **78**, 195424 (2008).

7. A. Lakhtakia and T. G. Mackay, "Classical electromagnetic model of surface states in topological insulators," J. Nanophoton. **10**, 033004 (2016).
8. M. Autore, F. D'Apuzzo, A. Di Gaspare, V. Giliberti, O. Limaj, P. Roy, M. Brahlek, N. Koirala, S. Oh, F. J. García de Abajo, and S. Lupi, "Plasmon-phonon interactions in topological insulator microrings," Adv. Opt. Mater. **3**, 1257–1263 (2015).
9. J. C. Granada E and D. F. Rojas, "Local excitations in thin metal films bounded by topological insulators," Physica B **455**, 82–84 (2014).
10. A. Karch, "Surface plasmons and topological insulators," Phys. Rev. B **83**, 245432 (2011).
11. Z.-M. Liao, B.-H. Han, H.-C. Wu, L. V. Yashina, Y. Yan, Y.-B. Zhou, Y.-Q. Bie, S. I. Bozhko, K. Fleischer, I. V. Shvets, Q. Zhao, and D.-P. Yu, "Surface plasmon on topological insulator/dielectric interface enhanced ZnO ultraviolet photoluminescence," AIP Adv. **2**, 022105 (2012).
12. J. Qi, H. Liu, and X. C. Xie, "Surface plasmon polaritons in topological insulators," Phys. Rev. B **89**, 155420 (2014).
13. M. I. D'yakonov, "New type of electromagnetic wave propagating at an interface," Sov. Phys. J. Exp. Theor. Phys. **67**, 714–716 (1988).
14. O. Takayama, L.-C. Crasovan, S. K. Johansen, D. Mihalache, D. Artigas, and L. Torner, "Dyakonov surface waves: a review," Electromagnetics **28**, 126–145 (2008).
15. O. Takayama, D. Artigas, and L. Torner, "Practical dyakonons," Opt. Lett. **37**, 4311–4313 (2012).
16. S. Vuković, J. J. Miret, C. J. Zapata-Rodríguez, and Z. Jakšić, "Oblique surface waves at an interface between a metal-dielectric superlattice and an isotropic dielectric," Phys. Scripta **T149**, 014041 (2012).
17. Y.-L. Zhang, Q. Zhang, and X.-Z. Wang, "Extraordinary surface polaritons in obliquely truncated dielectric/metal metamaterials," J. Opt. Soc. Am. B **33**, 543–547 (2016).
18. A. Lakhtakia and J. A. Polo, Jr., "Dyakonov-Tamm wave at the planar interface of a chiral sculptured thin film and an isotropic dielectric material," J. Eur. Opt. Soc. **2**, 07021 (2007).
19. I. Hodgkinson, Q. h. Wu, and J. Hazel, "Empirical equations for the principal refractive indices and column angle of obliquely deposited films of tantalum oxide, titanium oxide, and zirconium oxide," Appl. Opt. **37**, 2653–2659 (1998).
20. A. Lakhtakia and R. Messier, *Sculptured Thin Films: Nanoengineered Morphology and Optics* (SPIE, 2005), Chap. 7.
21. J. A. Polo, Jr., T. G. Mackay, and A. Lakhtakia, *Electromagnetic Surface Waves: A Modern Perspective* (Elsevier, 2013), Chap. 4.
22. C. F. Bohren and A. J. Hunt, "Scattering of electromagnetic waves by a charged sphere," Can. J. Phys. **55**, 1930–1935 (1977).
23. J. A. Polo, Jr., S. R. Nelatury, and A. Lakhtakia, "Propagation of surface waves at the planar interface of a columnar thin film and an isotropic substrate," J. Nanophoton. **1**, 013501 (2007).
24. A. H. Castro Neto, F. Guinea, N. M. R. Peres, K. S. Novoselov, and A. K. Geim, "The electronic properties of graphene," Rev. Mod. Phys. **81**, 109–162 (2009).
25. A. M. Nemilentsau, "Linear surface conductivity of an achiral single-wall carbon nanotube," J. Nanophoton. **5**, 050401 (2011).
26. R. Bouchendira, P. Cladé, S. Guellati-Khélifa, F. Nez, and F. Biraben, "New determination of the fine structure constant and test of the quantum electrodynamics," Phys. Rev. Lett. **106**, 080801 (2011).
27. M. Born and E. Wolf, *Principles of Optics*, 7th ed. (CUP, 1999), Chap. 15.